ACCSCIENCE PUBLISHING

International Journal of Bioprinting

ACCEPTED PAPER · MAIN TEXT

Mesenchymal stem cell differentiation in constructs fabricated by 3D bioprinting using a carboxyvinyl polymer-based support material

Article ID: IJB026200190

Citation: Kotani T, Sakai S. Mesenchymal stem cell differentiation in constructs fabricated by 3D bioprinting using a carboxyvinyl polymer-based support material. *Int J Bioprint*. 2026. doi: 10.36922/IJB026200190

AccScience Publishing
RESEARCH ARTICLE
Volume X Issue X (2026)
doi: 10.36922/IJB026200190

Mesenchymal stem cell differentiation in constructs fabricated by 3D bioprinting using a carboxyvinyl polymer-based support material

Running title: Behavioral evaluation of bioprinted MSCs

Takashi Kotani and Shinji Sakai*

Division of Chemical Engineering, Department of Materials Engineering Science, Graduate School of Engineering Science, The University of Osaka, Toyonaka, Osaka 560-8531, Japan

***Corresponding author:**
Shinji Sakai (sakai@cheng.es.osaka-u.ac.jp)

Citation: Kotani T, Sakai S. Mesenchymal stem cell differentiation in constructs fabricated by 3D bioprinting using a carboxyvinyl polymer-based support material. *Int J Bioprint.* 2026. doi: 10.36922/IJB026200190

Received: May 13, 2026
Revised: June 8, 2026
Accepted: June 10, 2026
Published online: June 10, 2026

Abstract

Three-dimensional bioprinting using a carboxyvinyl polymer (CVP) solution as a support material, alternately extruded with bioink, holds great promise for tissue engineering and regenerative medicine. This approach enables the fabrication of constructs that are sufficiently soft to preserve the functionality of enclosed cells. To evaluate the applicability of this support material and printing method for mesenchymal stem cells (MSCs), we examined the behavior of immortalized human bone marrow-derived MSCs (UE7T-13). This was carried out in constructs printed with bioinks containing 0.5 w/v% phenol-containing hyaluronic acid, 0.1 w/v% phenol-containing gelatin, and 10 U/mL horseradish peroxidase, which were crosslinked by hydrogen peroxide (H_2O_2) supplied from a support material composed primarily of CVP. During the 14 days of culture after printing, UE7T-13 cells enclosed in the printed constructs elongated and proliferated while maintaining high viability (>90%) and metabolic activity. Furthermore, antibody immunostaining revealed that the cells within the constructs maintained the characteristic MSC phenotype (CD44-positive and CD45-negative). Additionally, following osteogenic, adipogenic, and chondrogenic induction, the cells successfully produced lineage-associated products within the constructs, and the amounts of these products were controlled by varying the H_2O_2 concentration (1–10 mM) in the support material. Overall, the use of CVP together with H_2O_2 in the support material, combined with 3D bioprinting, effectively minimized adverse effects on MSC stemness and differentiation potential, while providing a practical strategy for regulating lineage-specific differentiation. These results demonstrate that this method enhances the utility of horseradish peroxidase-containing bioinks and offers great potential for tissue engineering applications.

Keywords: 3D bioprinting; Support material; Carboxyvinyl polymer; Mesenchymal stem cell; Phenol group

1. Introduction

Three-dimensional (3D) bioprinting, a technique for fabricating cell-laden hydrogel constructs based on digital designs, has become an essential technology in tissue engineering, regenerative medicine, and drug screening[1-3]. Among the various printing methods used with this technology, extrusion-based 3D bioprinting, which involves extruding a bioink through a nozzle or needle, is one of the most widely used[4, 5]. It enables the fabrication of multi-ink constructs and offers advantages in terms of compatibility with high-cell-density inks, adaptability to diverse materials, and enhanced cost-effectiveness[6, 7].

In extrusion-based 3D bioprinting, a bioink containing cells is typically deposited layer-by-layer onto a substrate and gelled to form a hydrogel construct[8]. In this printing method, during the fabrication of constructs soft enough to support cellular proliferation and function, the deposited ink tends to deform noticeably under its own weight[9, 10]. To address this issue, we previously developed a novel printing method employing a support material alternately extruded with bioink to induce gelation[11, 12]. In this method, the support material not only maintains the shape of the extruded bioink but also supplies the chemicals necessary for hydrogelation. This method not only enables the fabrication of constructs from inks that are difficult to print without support materials, but also solves the problem of construct deformation resulting from support material distortion in conventional embedded printing[11, 12]. The feasibility of this method in the field of 3D bioprinting has been demonstrated by printing cell-laden constructs with bioinks containing polymers with phenol groups (polymer-Phs)[11, 12].

Polymer-Ph solutions are attractive for providing stable hydrogels under physiological conditions through rapid, cell-friendly processes such as enzymatic crosslinking with horseradish peroxidase (HRP)[13, 14] and photo-crosslinking with ruthenium(II) tris-bipyridyl dication ($[Ru(bpy)_3]^{2+}$)[15, 16]. Through these crosslinking methods, cell-laden hydrogels composed of various polymers have been developed, including hyaluronic acid with phenol groups (HA-Ph)[17, 18], alginate[19, 20], chitosan[21, 22], poly(vinyl alcohol)[23, 24], gelatin (gelatin-Ph)[25, 26], other polysaccharides and proteins[27-29], and polysaccharide-protein complexes[14, 18, 26]. By utilizing these polymers as bioink materials in our current printing method that alternately extrudes support materials and bioinks, we have shown that soft constructs capable of supporting cell proliferation can be fabricated[11, 12]. Furthermore, the applicability of this printing method to stem cells was demonstrated in a study

using a bioink containing polymer-Ph and HRP, along with a support material that supplied the reaction substrate, hydrogen peroxide (H_2O_2)[30].

Bioprinting combined with stem cell technology has attracted attention as a promising approach for tissue engineering and regenerative medicine[31]. Among the various types of stem cells, mesenchymal stem cells (MSCs) are multipotent cells capable of self-renewal and differentiation into multiple cell types, including osteoblasts, chondrocytes, and adipocytes[32]. When applying extrusion-based 3D bioprinting to MSCs, the selection of support materials is a critical factor in addition to the composition of the bioink and printing parameters. Differences in osmolarity, residual components, and diffusion properties among various support materials can affect the microenvironment of cells enclosed in constructs, indicating potential implications for stemness maintenance and differentiation behaviors[31, 33]. Therefore, evaluating the influence of support-material-assisted bioprinting on the stemness and differentiation potential of MSCs is important in regenerative medicine.

Various support materials have been employed in bioprinting, including carboxyvinyl polymer (CVP) solutions[34-36], gelatin slurries[10], and starch slurries[30]. Among these, the CVP solution possesses several advantages, such as cytocompatibility, autoclave sterilizability[11], tunable rheological properties, and high reproducibility with minimal batch-to-batch variation. To the best of our knowledge, no study has investigated the effects of a CVP solution alternately extruded with bioink as a support material on stem cells.

This study aimed to evaluate the applicability of this printing method to MSCs, in which a CVP solution that promotes gelation is alternately extruded with a bioink. In a previous study on this method, a CVP-based gel for ultrasonographic examinations was supplemented with H_2O_2 and used as the support material, whereas a solution containing polymer-Ph, HRP, and cells was used as the bioink, and the effects of various factors on printability and cytocompatibility were evaluated[11]. In this study, we employed printing conditions and support materials in which both high printability and cytocompatibility were achieved; these materials were fabricated using bioinks containing HA-Ph, gelatin-Ph, and immortalized human bone marrow-derived mesenchymal stem cells (UE7T-13) (**Figure 1a**). UE7T-13 cells are widely used in tissue engineering and regenerative medicine[37-39]. Subsequently, during culture in basal media, the maintenance of stemness in the enclosed cells was evaluated based on their survival, morphology,

metabolic activity, and mesenchymal phenotypes. Furthermore, during culture in the differentiation medium, the maintenance of differentiation potential was evaluated based on lineage-associated products (**Figure 1b**).

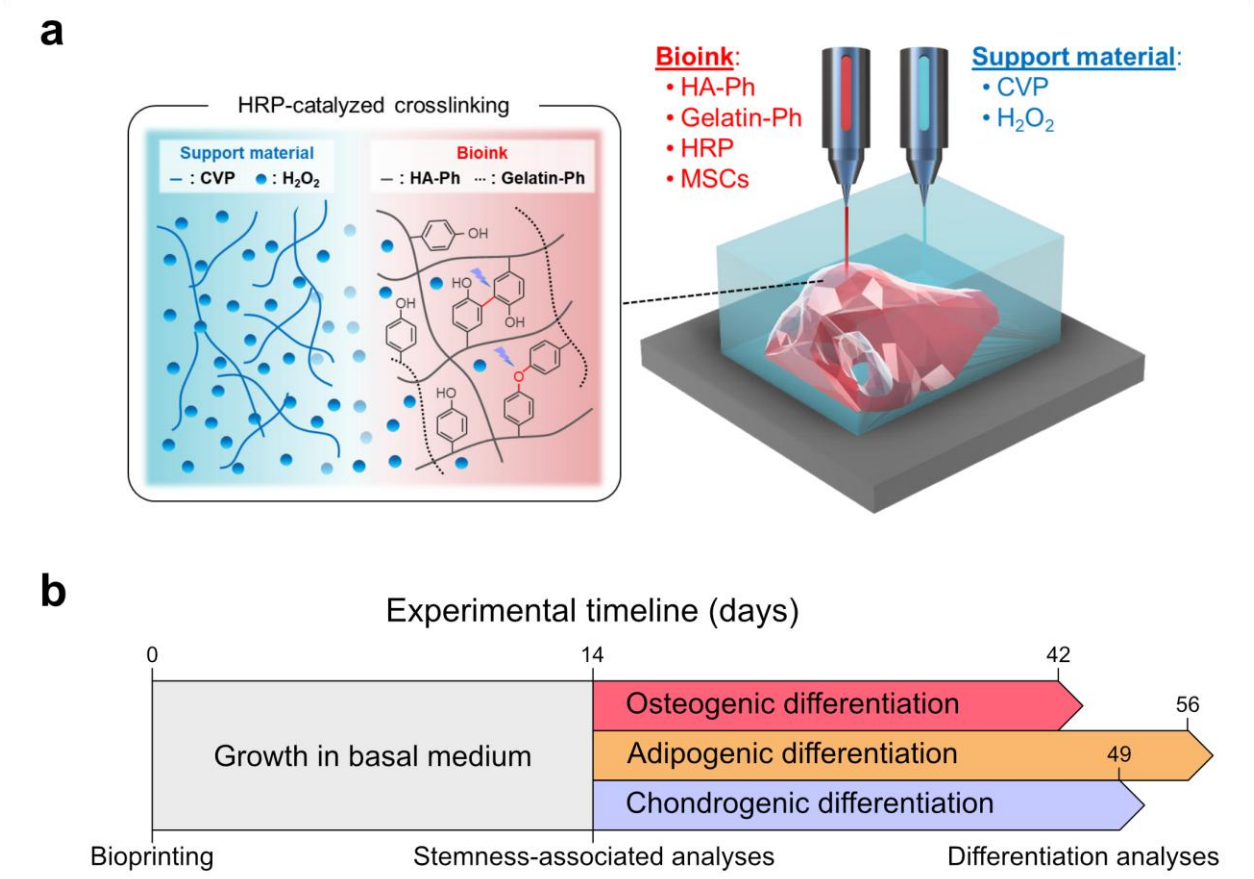

Figure 1. (a) Conceptual illustration of extrusion-based 3D bioprinting using support material containing CVP and H_2O_2 extruded with bioink containing HA-Ph, gelatin-Ph, HRP, and MSCs. (b) Experimental timeline for evaluating stemness-associated analyses and osteogenic, adipogenic, and chondrogenic differentiation of UE7T-13 cells enclosed in constructs.

2. Materials and methods

2.1. Materials

HA-Ph (1.5×10^{-4} mol-Ph/g of HA-Ph) and gelatin-Ph (1.3×10^{-4} mol-Ph/g of gelatin-Ph) were synthesized following a previously reported method[13, 40]. Tyramine (supplied as tyramine hydrochloride; Chem-Impex, Wood Dale, IL, USA) and 3-(4-hydroxyphenyl)propionic acid (Tokyo Chemical Industry, Tokyo, Japan) were respectively grafted onto hyaluronic acid (supplied as sodium hyaluronic acid, HA–LQ, average molecular weight: 850–1600 kDa; Kewpie, Tokyo, Japan) and gelatin (from bovine skin, gel-strength ~225 g Bloom, Type B; molecular weight not specified by the supplier; Sigma-Aldrich, St. Louis, MO, USA), using water-soluble carbodiimide hydrochloride (Peptide Institute, Osaka, Japan) and N-hydroxysuccinimide (FUJIFILM Wako Pure Chemical, Osaka, Japan). HRP, H_2O_2 aqueous solution (30 w/w%), hyaluronidase (from ovine testes, 1110 U/mg), catalase (from bovine liver, 8000 U/mg), and 4% paraformaldehyde phosphate buffer solution were purchased from FUJIFILM Wako Pure Chemical. A CVP-based gel for ultrasonographic examinations (Projelly, high-viscosity type; JEX, Osaka, Japan) was used as the support material. According to the product information provided by JEX, the solvent of the solution was purified water. The osteogenic differentiation medium was purchased from Cell Applications (San Diego, CA, USA). Media for adipogenic and chondrogenic differentiation were purchased from Lonza (Walkersville, MD, USA). Calcein-AM and propidium iodide (PI) were purchased from Nacalai Tesque (Kyoto, Japan) and Dojindo (Kumamoto, Japan), respectively.

2.2. Rheological properties

The rheological properties of 0.5 w/v% HA-Ph and 0.1 w/v% gelatin-Ph in phosphate-buffered saline (PBS, pH 7.4) were measured using a rheometer (HAAKE MARS III; Thermo Fisher Scientific, Waltham, MA, USA) at 25 ºC. The viscosity of the solution was measured for 360 s at shear rates ranging from 0.0001 to 1000 s^{-1} using a parallel-plate rheometer with a 30 mm radius and a 0.5 mm gap.

2.3. Diphenol formation

Diphenol formation in 100 µL hydrogels containing 0.5 w/v% HA-Ph, 0.1 w/v% gelatin-Ph, 0.1–10 U/mL HRP, and 1–10 mM H_2O_2 was measured using a fluorescence plate reader (SpectraMax iD3; Molecular Devices, San Jose, CA, USA) at approximately 25 ºC. Fifteen min after initiating

the crosslinking, fluorescence emission spectra from 350 to 600 nm were measured at an excitation wavelength of 310 nm. The peak at approximately 420 nm indicated diphenol formation.

2.4. Compressive stiffness of printed constructs

The compressive stiffness of printed constructs (8 mm diameter, 2 mm height) was measured using a material tester (EZ-SX; Shimadzu, Kyoto, Japan) equipped with a 5N load cell. The constructs were printed using an extrusion-based 3D bioprinter (BioX; Cellink, Gothenburg, Sweden) at approximately 25 ºC. PBS containing 0.5 w/v% HA-Ph, 0.1 w/v% gelatin-Ph, and 0.1–10 U/mL HRP was used as the ink. CVP-based gel containing 2.0 w/w% CVP and 1 or 10 mM H_2O_2 was used as the support material. The ink and support material were extruded from 27-gauge tapered nozzles at 2.8 μL/s for both the ink and support material. The thickness of each layer was set to 0.3 mm (first layer: 0.2 mm). Five min after printing, the support material was removed from the constructs. Young's modulus was calculated from the slope of the stress–strain curve in the strain range of 1–10% during compression at 6 mm/s using an 8 mm probe.

2.5. Cell culture

Immortalized human bone marrow-derived MSCs (UE7T-13; Riken Cell Bank, Ibaraki, Japan) were grown in Dulbecco's Modified Eagle Medium (DMEM; Shimadzu, Kyoto, Japan) containing 10 v/v% fetal bovine serum and 1 g/L glucose in a humidified 5% CO_2 incubator at 37 ºC.

2.6. 3D bioprinting with cells

A 3D bioprinter (BioX) was used to print cell-laden constructs (1 mm width, 1 mm height) (**Figure S1**). HA-Ph and gelatin-Ph were sterilized by ethanol treatment, dried, and dissolved in PBS overnight. Immediately before printing, HRP and UE7T-13 cells were added to the polymer solution to prepare the bioink containing 0.5 w/v% HA-Ph, 0.1 w/v% gelatin-Ph, 10 U/mL HRP, and 1×10^6 cells/mL UE7T-13 cells. The support materials were prepared by supplementing autoclaved CVP-based gel containing 2.0 w/w% CVP with H_2O_2 to final concentrations of 1 or 10 mM. The H_2O_2 solution used in this study was a commercially available 30 w/w% aqueous solution and was added aseptically to the autoclaved CVP-based gel. No additional sterilization was performed for the H_2O_2 solution. Using the nozzles and layer thickness described in Section 2.4, the bioink and support material were extruded at 5.2 and 1.6 μL/s, respectively. After removal of the support material 5 min after printing, the constructs were incubated overnight in 2 mL of

culture medium containing 1 mg/mL catalase to degrade the remaining H_2O_2 to water and oxygen. Thereafter, the medium was replaced with 2 mL of culture medium without catalase.

2.7. Live/dead staining

Cells in the constructs were stained with Calcein-AM and PI at final concentrations of 1.0 μg/mL each on days 1, 7, and 14 after printing. Stained cells were observed under a fluorescence microscope (APX-100; Olympus, Tokyo, Japan).

2.8. Mitochondrial activity

The mitochondrial activity of cells in the constructs was assessed using a reagent containing WST-8 (Cell Count Reagent SF; Nacalai Tesque, Kyoto, Japan) at 1, 7, and 14 days after printing. The cell-laden constructs were incubated in DMEM containing 10 v/v% of the reagent at 37 ºC for 3 h. After incubation, mitochondrial activity was quantified by measuring the absorbance at 450 nm using a UV-Vis spectrometer (UV-2600, Shimadzu).

2.9. Flow cytometry

Flow cytometry of cells within the constructs was conducted to assess CD44 and CD45 expression 14 days after printing. The cells were collected by degrading the constructs with incubation in DMEM containing 0.1 w/v% hyaluronidase at 37 ºC for 1.5 h. Then, the aggregates of the collected cells were dissociated by incubation in a 0.1 w/v% trypsin solution at 37 ºC for 10 min. The cells were stained with Calcein-AM, followed by incubation in a solution containing Human TruStain FcX™ (BioLegend, San Diego, CA, USA) at approximately 25 ºC for 10 min. Finally, the cells were stained with PerCP/Cyanine5.5-conjugated anti-mouse/human CD44 (BioLegend) and BD Horizon™ PE-CF594-conjugated mouse anti-human CD45 (BD Biosciences, Franklin Lakes, NJ, USA) for 30 min at 4 ºC. Flow cytometry was conducted using a CytoFLEX flow cytometer (Beckman Coulter, Brea, CA, USA).

2.10. Osteogenic, adipogenic, and chondrogenic differentiation induction

Osteogenic, adipogenic, and chondrogenic differentiation of cells in the constructs was induced by replacing DMEM with the corresponding differentiation media 14 days after printing.

2.11. Alizarin red staining

Alizarin red staining was performed 14 and 28 days after the initiation of osteogenic differentiation. The cells in the constructs were fixed with paraformaldehyde at approximately 25 ºC for 30 min. Subsequently, the calcium deposits in the constructs were stained with water containing 40 mM Alizarin Red S (FUJIFILM Wako Pure Chemical) for 1 h, followed by washing with water. The calcium deposits were observed using a microscope (APX-100).

2.12. Alkaline phosphatase (ALP) activity

The ALP activity of cells in the constructs was measured at 1, 14, and 28 days after the initiation of osteogenic differentiation, following a previously reported method[30]. After collection, as described in Section 2.9, the cells were lysed with 50 mM 2-amino-2-methyl-1-propanol buffer containing 0.1 v/v% Triton X-100 (Nacalai Tesque) at 4 ºC for 10 min. After centrifugation at 12,000 × *g* for 10 min at 4 ºC, lysates were incubated with 5 mM disodium p-nitrophenyl phosphate (FUJIFILM Wako Pure Chemical) in 2-amino-2-methyl-1-propanol buffer at 37 ºC for 1 h. The resulting p-nitrophenolate (pNP) concentration was determined from the absorbance at 405 nm using a UV-Vis spectrometer (UV-2600).

2.13. Oil Red O staining

Oil Red O staining was performed at 7, 24, and 42 days after the initiation of adipogenic differentiation. After fixing the cells as described in Section 2.11, lipid droplets in the constructs were stained with a 60 v/v% 2-propanol solution containing 0.3 w/v% Oil Red O (Sigma-Aldrich) for 30 min, followed by washing with a 60 v/v% 2-propanol solution. Lipid droplets were observed under a microscope (APX-100).

2.14. Alcian blue staining

Alcian blue staining was performed at 21 and 35 days after the initiation of chondrogenic differentiation. After fixing the cells as described in Section 2.11, sulfated glycosaminoglycans in the constructs were stained with Alcian blue solution (FUJIFILM Wako Pure Chemical) for 30 min, followed by washing with HCl solution. Glycosaminoglycans were observed under a microscope (APX-100).

2.15. Structural stability of constructs

Structural stability was evaluated based on construct width retention during culture. Digital images were acquired at the indicated time points, and the average width of six sides was normalized to the value for the same construct on day 1.

2.16. Statistical analysis

The quantitative data are expressed as means with standard deviation. Microsoft Excel for Microsoft 365 MSO (Version 2605, Build 16.0.20026.20140, 64-bit; Microsoft, Redmond, WA, USA) was used for the statistical data analysis. Data were analyzed using one-way analysis of variance with Tukey's Honest Significant Difference (HSD) test. Differences were considered significant if the *P*-value was < 0.05.

3. Results and Discussion

3.1. Evaluation of viability, morphology, and proliferation of stem cells in a printed construct

We fabricated constructs containing UE7T-13 cells using a printing method that alternately extruded a bioink and a support material containing CVP and 1 mM or 10 mM H_2O_2, and evaluated the viability, morphology, and proliferation of the enclosed cells. Fluorescence microscopy showed that most Calcein-AM-stained cells exhibited green fluorescence over 14 days after printing (**Figure 2a**). On day 1 of culture, the cells displayed a predominantly round morphology; however, from day 7 onward, they adopted an elongated shape (**Figure 2a**). Furthermore, mitochondrial activity per construct increased during the 14 days of culture (**Figure 2b**). Additionally, there were no significant differences in cell survival, morphology, or mitochondrial activity within the constructs printed with support materials containing 1 and 10 mM H_2O_2. These results indicate that, in constructs printed with both H_2O_2 concentrations, cells elongated and proliferated while maintaining high viability and metabolic activity. Because construct properties can affect cell behavior, we characterized their compressive stiffness and diphenol formation. At 10 U/mL HRP, increasing the H_2O_2 concentration from 1 to 10 mM significantly increased Young's modulus from 1.3 ± 0.5 to 4.2 ± 1.8 kPa ($P < 0.05$, $n = 3$; **Figure S2**). In contrast, decreasing the HRP concentration to 0.1 U/mL reduced Young's modulus (**Figure S2**). Higher HRP and/or H_2O_2 concentrations also increased diphenol formation (**Figure S3**), consistent with previous reports[11, 41]. These results suggest that the increased reaction rate at higher HRP concentrations and the greater H_2O_2 supply increased the crosslinking density of the constructs.

Despite the increase in Young's modulus at higher H_2O_2 concentrations, the constructs remained sufficiently soft to allow cell elongation and proliferation. The observed cell elongation and proliferation are consistent with previously reported studies on UE7T-13 cells enclosed in hydrogels containing polymers with cell-adhesive motifs, such as gelatin, and characterized by mechanical properties too weak to support self-standing structures[30]. In addition to the cell adhesiveness and poor mechanical properties of the constructs, the use of a low-viscosity pseudoplastic bioink (**Figure S4**) similar to that employed in previous studies[11, 12], is thought to reduce the mechanical stress, including shear stress and pressure, on the cells during extrusion. This is particularly important for MSCs because of their sensitivity to such mechanical stimuli[42]. Overall, these results suggest that the printing method involving a support material containing CVP and H_2O_2 was compatible with MSCs and provided sufficiently soft constructs that supported cell survival, elongation, and proliferation.

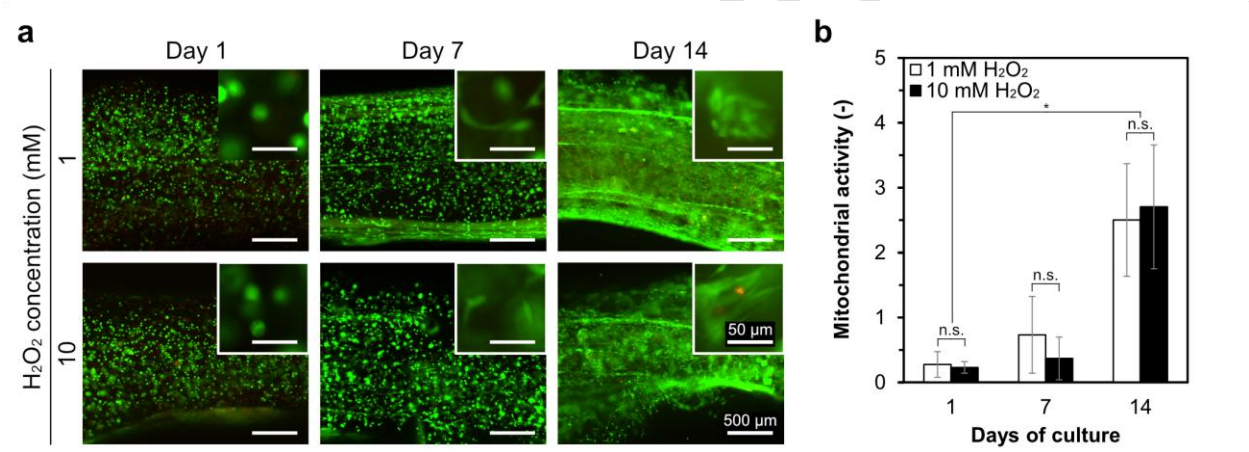

Figure 2. (a) Fluorescence images and (b) mitochondrial activity of UE7T-13 cells within constructs containing 0.5 w/v% HA-Ph and 0.1 w/v% gelatin-Ph on day 1, 7, and 14 of culture. The cells were stained using Calcein-AM (green: live cells) and PI (red: dead cells). The concentrations of HRP in the bioink, CVP, and H_2O_2 in the support material were 10 U/mL, 2.0 w/w%, and 1–10 mM, respectively. Error bars indicate standard deviation (n = 3). n.s.: no significant difference ($P > 0.05$), *$P < 0.05$, Tukey's HSD.

3.2. Evaluation of mesenchymal phenotype

We evaluated the effects of a printing process involving support materials containing CVP and H_2O_2, followed by 14 days of in situ culture within the constructs, on the mesenchymal phenotype

of UE7T-13 cells. As indicated in Section 3.1, cells were exposed to mechanical stress caused by extrusion and chemical stress caused by CVP and H_2O_2. Furthermore, the microenvironment within constructs may limit the diffusion of nutrients and oxygen. It has been suggested that these mechanical and chemical stresses, as well as the microenvironment characterized by low nutrient levels and hypoxia, affect the natural phenotypes of MSCs[42-44]. CD44 was selected as a positive marker to confirm the maintenance of the mesenchymal phenotype in the cells. CD44 plays a role in maintaining stem cell properties by binding to hyaluronic acid and promoting its adhesion, migration, and self-renewal[45]. Therefore, a decrease in CD44 expression indicates a deviation from the natural MSC phenotype. Additionally, the hematopoietic marker CD45 was selected as a negative marker, which is also a standard flow cytometry marker used in combination with CD44 to confirm MSC maintenance[32, 33, 46].

In both fluorescence imaging and flow cytometry, fluorescence derived from immunostained CD44 was observed on the surfaces of cells cultured in dishes and within the constructs (**Figure 3a, b**). In contrast, no CD45 fluorescence was observed (**Figure 3a, c**). Furthermore, the flow cytometry results indicated that cells cultured within the constructs exhibited higher CD44 expression than those cultured in dishes (**Figure 3b**). This increase in CD44 expression is thought to be due to the interaction between hyaluronic acid in the construct and the cell surface[47, 48]. However, no increase in CD44 expression was observed in UE7T-13 cells cultured in a hydrogel that did not contain hyaluronic acid[30]. Taken together with the results in Section 3.1, these findings indicate that the printing process using a support material containing CVP and H_2O_2 had no significant adverse effects on the stem cell properties of MSCs, including their natural morphology, proliferation potential, and phenotype. Furthermore, the enclosed MSCs were maintained undifferentiated for 14 days after printing.

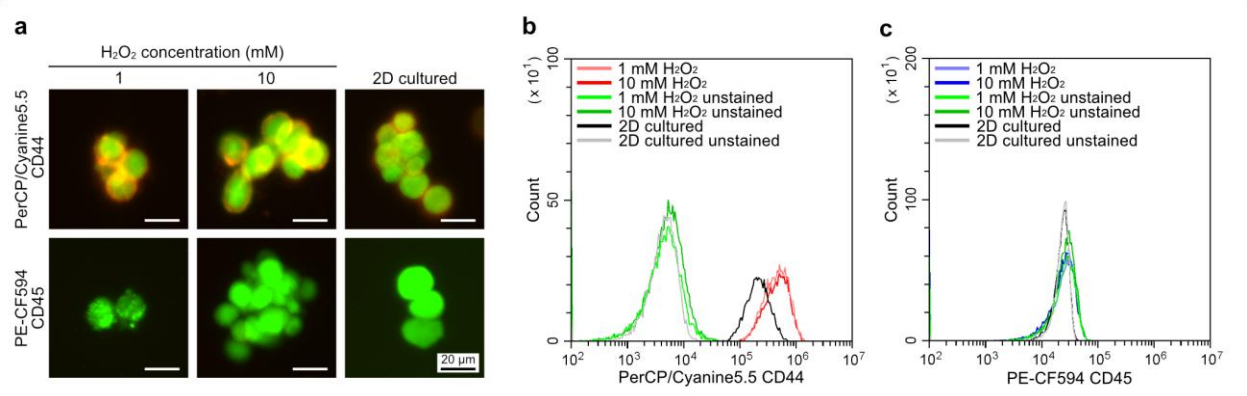

Figure 3. (a) Fluorescence images and (b, c) flow cytometry of UE7T-13 cells immunostained with CD44-PerCP/Cyanine 5.5 and CD45-PE-CF594. The cells were cultured in constructs or dishes for 14 days after printing and stained with Calcein-AM. The concentrations of HRP in the bioink, and CVP and H_2O_2 in the support material were 10 U/mL, 2.0 w/w%, and 1–10 mM, respectively.

3.3. Evaluation of osteogenic differentiation

To confirm that the UE7T-13 cells retained their differentiation potential even after 14 days of culture in the constructs, we evaluated their osteogenic differentiation potential. Osteogenic differentiation was induced for 28 days by replacing the basal medium with the differentiation induction medium on day 14 (**Figure 1b**). The progression of osteogenic differentiation was evaluated using Alizarin Red staining and ALP activity.

In constructs fabricated with support materials containing 1 and 10 mM H_2O_2, calcium deposition stained with alizarin red was observed throughout the constructs by day 14 of differentiation induction, and the staining intensity showed little change thereafter (**Figure 4a**). This result indicated that calcium deposition progressed rapidly during the first 14 days of induction and subsequently plateaued. The deposits exhibited a nodular morphology, consistent with the characteristics reported in previous studies on the osteogenic differentiation of UE7T-13 cells[38, 49]. No calcium deposition was observed in non-induced cells even after 42 days of culture (**Figure 4b**). In addition to calcium deposition, we evaluated the activity of ALP, a marker of osteogenic differentiation that is essential for calcification. ALP hydrolyzes phosphate esters to produce inorganic phosphates for hydroxyapatite formation. ALP activity per cell was assessed by measuring the absorbance of pNP, which is generated from p-nitrophenyl phosphate, after normalization to the total protein content. In cells subjected to osteogenic induction for 14 days, the absorbance of pNP was higher than that in non-induced cells (**Figure 4c**). Furthermore, pNP absorbance increased further when induction was continued for 28 days. In contrast, the absorbance of non-induced cells did not change even after 42 days of culture (**Figure 4c**). These results indicate that ALP activity was higher in differentiation-induced cells than in non-induced cells, and that it continued to increase throughout the induction period. Furthermore, from day 14 of induction onward, the constructs printed with 1 mM H_2O_2 exhibited higher ALP activity than those printed with 10 mM H_2O_2 (**Figure 4c**).

The continued increase in the ALP activity of UE7T-13 cells even after 14 days of differentiation induction, despite the absence of further expansion of the mineralized area, suggests that matrix maturation and mineralization processes remained active after the initial mineral deposition stage. Furthermore, the higher ALP activity observed in constructs printed with lower H_2O_2 concentrations is thought to be due to the lower crosslinking density of the construct, which provided an environment in which the cells could elongate more freely. Previous studies have shown that ALP activity increases in hydrogels with higher porosity and softer mechanical properties, which allows cells to elongate[50, 51]. Overall, these results from alizarin red staining and ALP activity measurements demonstrate that the 3D printing processes using support materials containing CVP and H_2O_2, as well as the culture period prior to differentiation induction, did not compromise the osteogenic potential of UE7T-13 cells or cause any unintended differentiation. Furthermore, these findings indicate that by controlling the H_2O_2 concentration, it is possible to modulate the crosslinking density of the constructs and the cellular microenvironment, thereby regulating osteogenic differentiation.

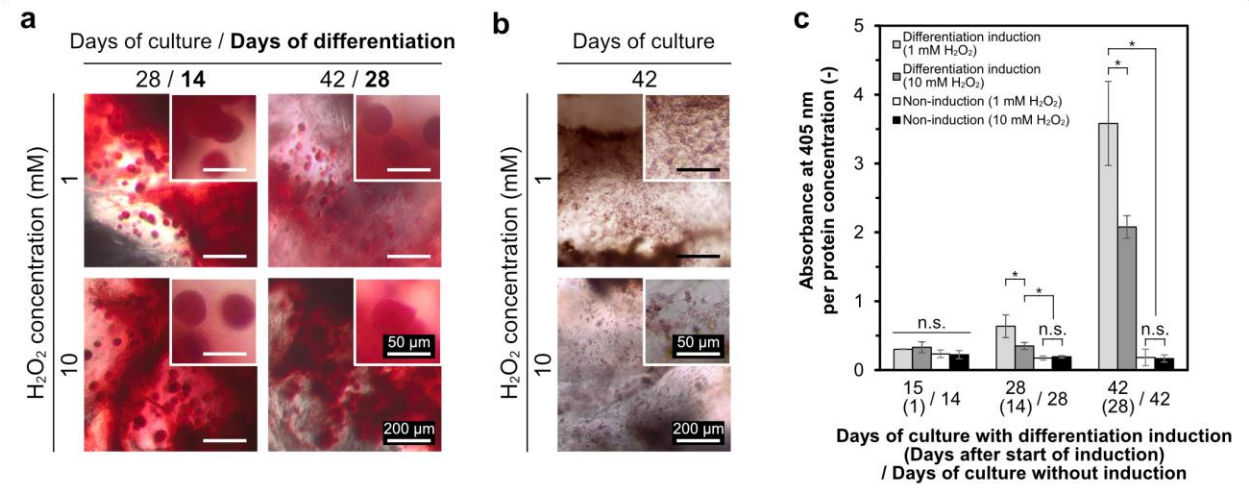

Figure 4. Assessment of osteogenic differentiation of the cells: alizarin red staining (a) with and (b) without differentiation induction, and (c) ALP activity per 1 mg/mL protein. Differentiation was conducted after an initial 14 days of enclosure. The concentrations of HRP in the bioink, CVP, and H_2O_2 in the support material were 10 U/mL, 2.0 w/w%, and 1–10 mM, respectively. Error bars: standard deviation ($n = 3$). n.s.: no significant difference ($P > 0.05$), *$P < 0.05$, Tukey's HSD.

3.4. Evaluation of adipogenic differentiation

We evaluated the adipogenic differentiation potential of UE7T-13 cells using these constructs. Adipogenic differentiation was induced using a differentiation medium from day 14 following printing, and was continued for 42 days (**Figure 1b**). On days 7, 24, and 42 after induction, adipogenic differentiation was evaluated by observing the lipid droplets associated with adipocyte differentiation using Oil Red O staining, the most common staining method for adipogenically differentiated MSCs[42]. On day 7 of induction, lipid droplets with diameters of less than 10 μm were observed, indicating the initiation of adipogenic differentiation (**Figure 5a**). By day 24, the diameters of some lipid droplets increased to 10 μm or more, and they formed aggregates in parts of the constructs. On day 42, they were distributed throughout the construct. These results indicated that the UE7T-13 cells enclosed in the constructs retained their adipogenic differentiation potential, successfully differentiated into the adipocyte lineage, and continued to undergo adipogenesis through day 42. In contrast, cells cultured in a basal medium for the same period formed almost no lipid droplets (**Figure 5b**). This result suggests that unwanted differentiation was not initiated by the printing process or cultivation within the construct before the induction of differentiation. Furthermore, on day 42, larger and more coalesced lipid droplets formed in the construct printed using a support material containing 1 mM H_2O_2 than in the construct printed using 10 mM H_2O_2. This result is consistent with previous reports and suggests that differentiation into adipocytes is promoted by softer constructs[52]. Overall, these results demonstrate that the printing process minimized adverse effects on the ability of cells to differentiate into adipocytes. As in the case of osteogenic differentiation described in Section 3.3, adjusting the H_2O_2 concentration can serve as a practical strategy for fabricating soft constructs that promote adipogenic differentiation.

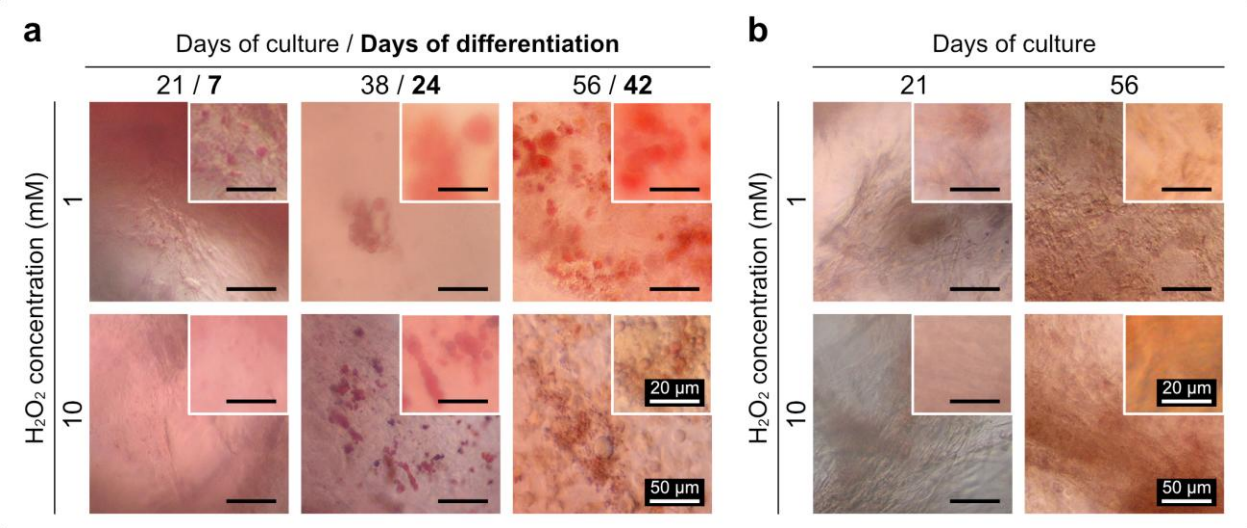

Figure 5. Adipogenic differentiation of UE7T-13 cells enclosed in constructs containing 0.5 w/v% HA-Ph and 0.1 w/v% gelatin-Ph. Micrographs of lipid droplets stained with Oil Red O (a) with and (b) without differentiation induction. Differentiation induction was started 14 days after bioprinting. The concentrations of HRP in the bioink, CVP, and H_2O_2 in the support material were 10 U/mL, 2.0 w/w%, and 1–10 mM, respectively.

3.5. Evaluation of chondrogenic differentiation

We evaluated the chondrogenic differentiation potential of the UE7T-13 cells enclosed in these constructs. Chondrogenic differentiation was induced with chondrogenic differentiation medium from day 14 following printing, continued for 35 days, and evaluated by observing the sulfated glycosaminoglycans produced via Alcian blue staining on days 21 and 35 after induction (**Figure 1b**). Alcian blue-stained microscopic aggregates were observed within the constructs on day 21, indicating the initial deposition of sulfated glycosaminoglycans (**Figure 6a**). Furthermore, by day 35, both the stained area and staining intensity increased, indicating the progression of glycosaminoglycan deposition. In contrast, no deposition was observed when the cells were cultured in a basal medium for the same period (**Figure 6b**). These results indicate that, similar to osteogenesis and adipogenesis, the printing process and culturing within the construct prior to differentiation induction did not cause any unintended differentiation before induction. Constructs printed using 1 mM H_2O_2 exhibited higher staining intensity at both time points than those printed using 10 mM, suggesting enhanced glycosaminoglycan formation in constructs with a lower crosslinking density. Consistent with previously reported findings, this result suggested that chondrogenic differentiation was enhanced in constructs with lower crosslinking density[53]. Based

on these results, similar to the findings for osteogenic and adipogenic differentiation, this printing process preserved the chondrogenic differentiation potential of UE7T-13 cells and demonstrated that the modulation of H_2O_2 concentration could regulate lineage-specific microenvironments for chondrogenic differentiation.

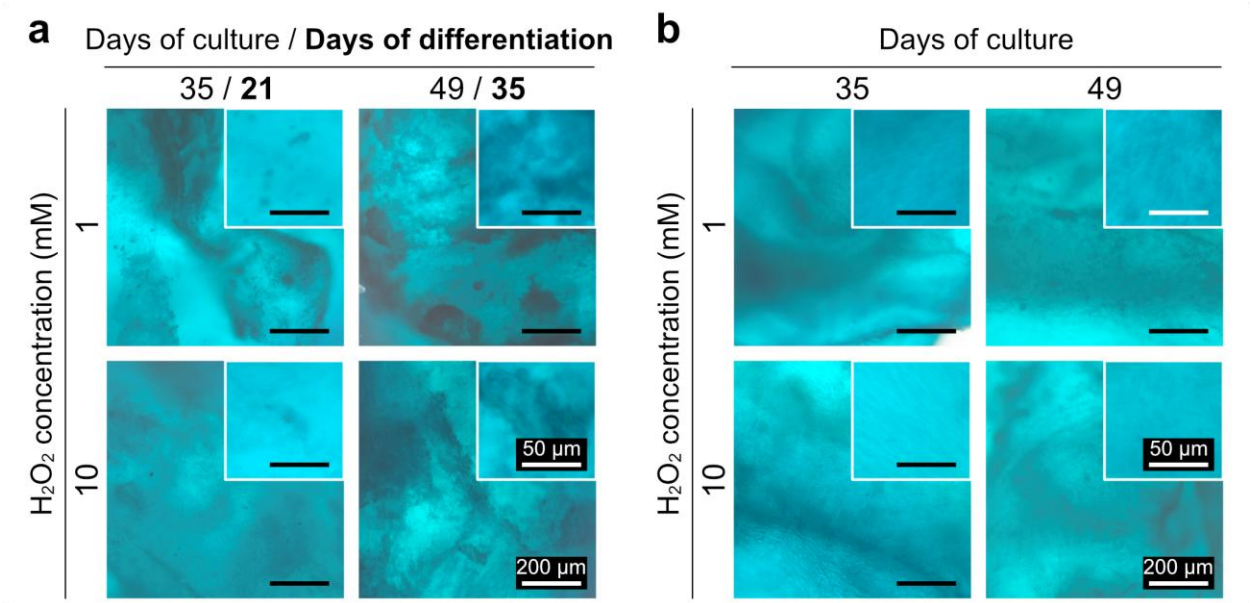

Figure 6. Chondrogenic differentiation of UE7T-13 cells enclosed in constructs containing 0.5 w/v% HA-Ph and 0.1 w/v% gelatin-Ph. Micrographs of sulfated glycosaminoglycans stained with alcian blue (a) with and (b) without differentiation induction. Differentiation induction was started 14 days after bioprinting. The concentrations of HRP in the bioink, CVP, and H_2O_2 in the support material were 10 U/mL, 2.0 w/w%, and 1–10 mM, respectively.

3.6. Structural stability of constructs

Structural stability was evaluated by measuring construct width during culture and normalizing it to its width on day 1. Regardless of the presence or absence of cells, the constructs did not collapse in the culture medium during the 14-day culture period, and their widths remained unchanged. However, deformation was observed only in the cell-laden constructs on day 14 (**Figure 7a–c**). This was likely due to an increase in tensile force associated with cell proliferation[54, 55]. The construct deformed more markedly during osteogenic differentiation induced from day 14 after printing and shrank significantly (**Figure 7d**). This shrinkage is thought to result from an increase in the actomyosin contractile force and cytoskeletal tension associated with osteogenic differentiation. No further shrinkage was observed after 14 days of osteogenic induction. This

result is likely due to the rapid progression of osteogenic differentiation in UE7T-13 cells during the first 14 days of induction, which is consistent with the calcium deposition results described in Section 3.4. In contrast, constructs subjected to chondrogenic differentiation exhibited less deformation than those subjected to osteogenic differentiation. This deformation was further reduced in constructs printed using support materials containing 10 mM H_2O_2, which produced a higher crosslinking density than 1 mM H_2O_2 (**Figure 7d**). Furthermore, the deformation was smaller during adipogenic differentiation (**Figure 7d**). This is consistent with the results of previous studies, which showed that adipogenic differentiation does not markedly increase cellular tensile force, whereas that of chondrocytes is higher than that of adipocytes but lower than that of osteocytes[56]. Overall, the results demonstrated that during the 14-day culture period prior to the induction of differentiation, the constructs remained structurally stable and similar to those without cells. In contrast, the subsequent induction of differentiation causes deformation corresponding to lineage-dependent cellular contractility.

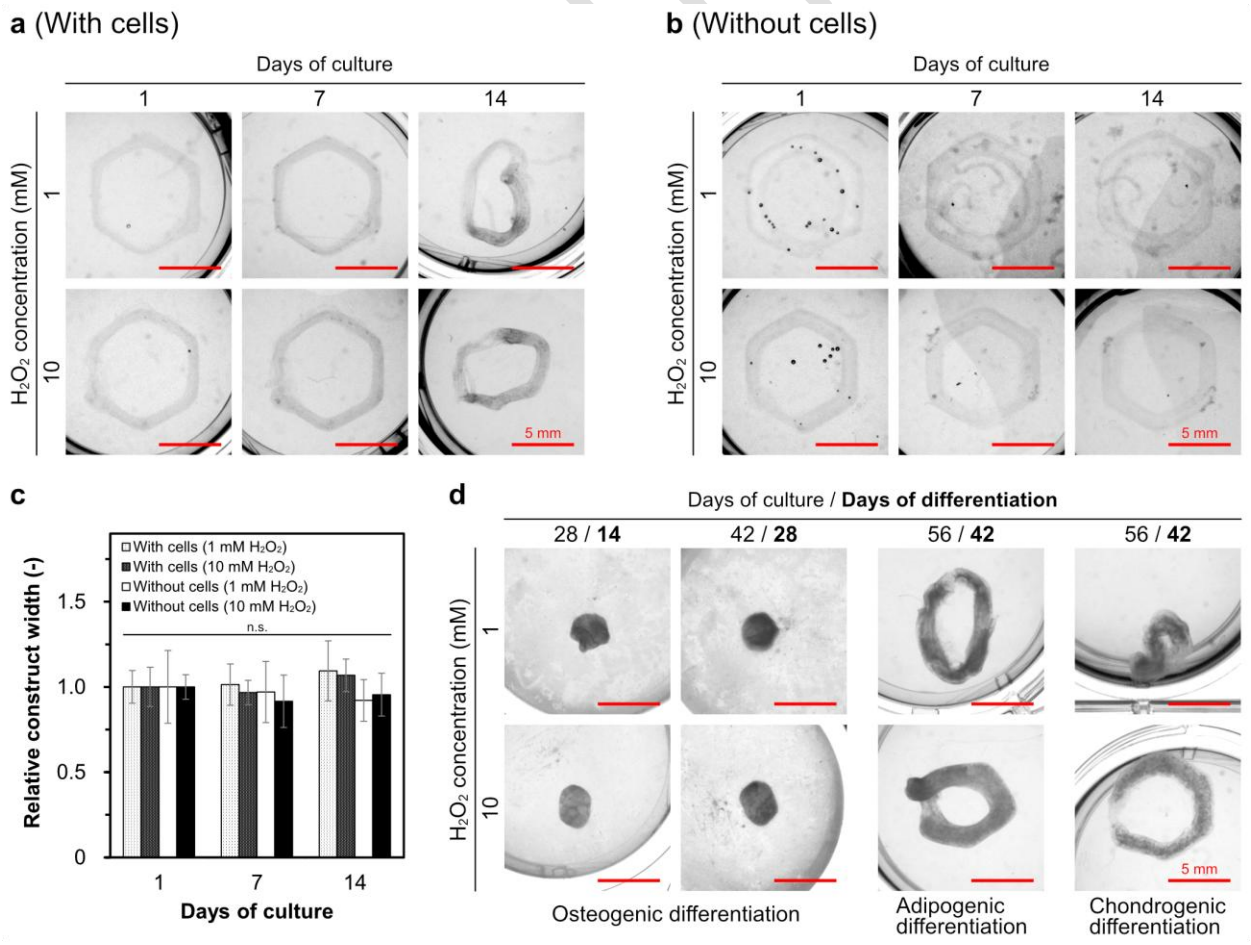

Figure 7. (a, b) Digital images and (c) relative width of constructs comprising 0.5 w/v% HA-Ph, 0.1 w/v% gelatin-Ph, 10 U/mL HRP (a) with and (b) without 1×10^6 cells/mL UE7T-13 cells. (d) Digital images of cell-laden constructs after osteogenic, adipogenic, and chondrogenic differentiation induction. The concentrations of HRP in the bioink, CVP, and H_2O_2 in the support material were 10 U/mL, 2.0 w/w%, and 1–10 mM, respectively. The construct width was calculated from the average widths of six sides of each construct and normalized to the width of the same construct on day 1. Error bars: standard deviation (n = 6). n.s.: no significant difference ($P > 0.05$), Tukey's HSD.

3.7. Advantages, limitations, and future research

One of the advantages of this printing method is that H_2O_2 is spatially separated from the cell-laden bioink before extrusion. Because direct addition of H_2O_2 to polymer-Ph/HRP inks can cause gelation before extrusion, H_2O_2 delivery from the CVP-based support material allows the bioink to remain printable while inducing crosslinking after deposition[30]. In this system, the support material therefore functions both as a temporary structural support and as a H_2O_2 supplier.

Compared with our previous studies using this printing method[11], the present study focuses on the behavior of MSCs within printed constructs. By evaluating cell morphology, proliferation, mesenchymal phenotype, and lineage-specific differentiation, this study demonstrates that the CVP/H_2O_2-based support material provides a soft microenvironment suitable for MSC behavior. In addition, changing the H_2O_2 concentration enabled modulation of construct properties and MSC differentiation behavior.

Although 3D bioprinting using support materials containing CVP and H_2O_2 has demonstrated potential applications in MSCs, several challenges remain. One such challenge, as previously reported, is the difficulty of fabricating thick or structurally homogeneous constructs[12]. This is because the diffusion of chemicals for crosslinking becomes limited as the distance from the support material increases, resulting in a decrease in crosslinking density within the construct[12]. Consequently, spatial heterogeneity in cellular differentiation may occur within these constructs[33]. Furthermore, the relative contributions of matrix stiffness, porosity, and nutrient and oxygen transport to the observed differentiation behavior remain unclear. We believe this issue can be partially resolved by adjusting the crosslinking density by optimizing the H_2O_2 concentration in the support material, as well as the HA-Ph and gelatin-Ph concentrations in the bioink.

Additionally, as described in Section 3.6, soft constructs fabricated using this printing method face the challenge of significant shrinkage due to cellular contractile forces during lineage-specific differentiation. This shrinkage impedes the diffusion of oxygen, nutrients, and growth factors required for cell survival and differentiation[54]. To address this issue, one possible approach is to incorporate a second ink containing polymer-Ph and HRP, which forms a hydrogel stiffer than the cell-laden regions, into the construct. This is expected to provide structural support that suppresses deformation of the construct. Overall, the potential of this method for applications in tissue engineering is likely to improve through optimizations of printing conditions and compositions of the ink and support material, along with the incorporation of additional functional inks for structural support. This will enable the fabrication of constructs that are better suited for MSC-based tissue engineering research while minimizing adverse effects on MSCs.

4. Conclusion

To evaluate the applicability of an extrusion-based 3D bioprinting method for MSCs, in which a support material containing CVP and H_2O_2 was extruded alternately with a bioink, we assessed the stemness and differentiation potential of UE7T-13 cells enclosed in printed constructs. During the 14-day culture period prior to the induction of differentiation, the cells elongated and proliferated within the constructs while maintaining high viability and metabolic activity. Furthermore, these cells retained their mesenchymal phenotype throughout the culture period. Following osteogenic, adipogenic, and chondrogenic induction, the cells successfully produced lineage-associated products, and the amounts of these products were controlled by varying the H_2O_2 concentration in the support materials. Overall, the extrusion-based 3D bioprinting method using a support material containing CVP and H_2O_2 minimized the adverse effects on the stemness and differentiation potential of MSCs and provided a practical strategy for regulating lineage-specific differentiation, highlighting its potential for stem cell-based 3D bioprinting applications. Future optimization to address these limitations and the integration of multiple bioinks may further broaden the applicability of bioinks that mainly contain polymer-Ph and HRP for tissue engineering and regenerative medicine applications.

Acknowledgments
The authors acknowledge JEX Co., Ltd. for helpful technical assistance regarding product material information. The authors also thank Colin Zhang for his assistance with English language editing.

Funding
This study was financially supported by the Adaptable and Seamless Technology Transfer Program through Target-driven R&D (A-STEP) of the Japan Science and Technology Agency (JST), Japan Grant Number JPMJTR234C and JSPS KAKENHI Grant Number JP24KJ1658.

Conflict of interest
The authors declare they have no competing interests.

Author contributions
Conceptualization: Takashi Kotani, Shinji Sakai
Data curation: Takashi Kotani
Formal analysis: Takashi Kotani
Funding acquisition: Takashi Kotani, Shinji Sakai
Investigation: Takashi Kotani
Methodology: Takashi Kotani, Shinji Sakai
Supervision: Shinji Sakai
Visualization: Takashi Kotani
Writing–original draft: Takashi Kotani
Writing–review & editing: Takashi Kotani, Shinji Sakai

Ethics approval and consent to participate
Not applicable.

Consent for publication
Not applicable.

References

1. Klebe RJ, 1988, Cytoscribing: a method for micropositioning cells and the construction of two- and three-dimensional synthetic tissues. Exp. Cell Res., 179(2): 362-373.

https://doi.org/10.1016/0014-4827(88)90275-3.
2. Mironov V, Boland T, Trusk T, *et al.*, 2003, Organ printing: computer-aided jet-based 3D tissue engineering. Trends Biotechnol., 21(4): 157-161.

https://doi.org/10.1016/S0167-7799(03)00033-7.
3. Nakamura M, Iwanaga S, Henmi C, *et al.*, 2010, Biomatrices and biomaterials for future developments of bioprinting and biofabrication. Biofabrication, 2(1): 014110.

https://doi.org/10.1088/1758-5082/2/1/014110.
4. Holland I, 2025, Extrusion bioprinting: meeting the promise of human tissue biofabrication? Prog Biomed Eng (Bristol), 7(2): 023001.

https://doi.org/10.1088/2516-1091/adb254.
5. Kazemi M, Maralbashi S, 2025, Advances in 3D bioprinting for medical application: opportunities and challenges. Biomed Eng Online, 25(1): 11.

https://doi.org/10.1186/s12938-025-01498-y.
6. Frost BA, Sutliff BP, Thayer P, *et al.*, 2019, Gradient Poly(ethylene glycol) Diacrylate and Cellulose Nanocrystals Tissue Engineering Composite Scaffolds via Extrusion Bioprinting. Front. Bioeng. Biotechnol., 7: 280.

https://doi.org/10.3389/fbioe.2019.00280.
7. Daly AC, Prendergast ME, Hughes AJ, *et al.*, 2021, Bioprinting for the Biologist. Cell, 184(1): 18-32.

https://doi.org/10.1016/j.cell.2020.12.002.
8. Tejada Jacob G, Passamai VE, Katz S, *et al.*, 2022, Hydrogels for extrusion-based bioprinting: General considerations. Bioprinting, 27: e00212.

https://doi.org/10.1016/j.bprint.2022.e00212.
9. Shiwarski DJ, Hudson AR, Tashman JW, *et al.*, 2021, Emergence of FRESH 3D printing as a platform for advanced tissue biofabrication. APL Bioeng, 5(1): 010904.

https://doi.org/10.1063/5.0032777.
10. Hinton TJ, Jallerat Q, Palchesko RN, *et al.*, 2015, Three-dimensional printing of complex biological structures by freeform reversible embedding of suspended hydrogels. Sci Adv, 1(9): e1500758.

https://doi.org/10.1126/sciadv.1500758.
11. Kotani T, Mubarok W, Hananouchi T, *et al.*, 2023, Horseradish Peroxidase-Mediated Bioprinting via Bioink Gelation by Alternately Extruded Support Material. ACS Biomater Sci Eng, 9(10): 5804-5812.

https://doi.org/10.1021/acsbiomaterials.3c00996.
12. Kotani T, Hananouchi T, Sakai S, 2025, Enhancing visible light-induced 3D bioprinting: alternating extruded support materials for bioink gelation. Biomed Mater, 20(3): 035005.

https://doi.org/10.1088/1748-605X/adc0d6.
13. Kurisawa M, Chung JE, Yang YY, *et al.*, 2005, Injectable biodegradable hydrogels composed of hyaluronic acid-tyramine conjugates for drug delivery and tissue engineering. Chem Commun (Camb), (34): 4312-4314.

https://doi.org/10.1039/b506989k.
14. Sakai S, Matsuyama T, Hirose K, *et al.*, 2010, In situ simultaneous protein-polysaccharide bioconjugation and hydrogelation using horseradish peroxidase. Biomacromolecules, 11(5): 1370-1375.

https://doi.org/10.1021/bm1001608.
15. Fancy DA, Kodadek T, 1999, Chemistry for the analysis of protein-protein interactions: rapid and efficient cross-linking triggered by long wavelength light. Proc Natl Acad Sci U S A, 96(11): 6020-6024.

https://doi.org/10.1073/pnas.96.11.6020.
16. Elvin CM, Brownlee AG, Huson MG, *et al.*, 2009, The development of photochemically crosslinked native fibrinogen as a rapidly formed and mechanically strong surgical tissue sealant. Biomaterials, 30(11): 2059-2065.

https://doi.org/10.1016/j.biomaterials.2008.12.059.

17. Lee F, Chung JE, Kurisawa M, 2008, An injectable enzymatically crosslinked hyaluronic acid- hydrogel system with independent tuning of mechanical strength and gelation rate. Soft Matter, 4(4): 880-887.

https://doi.org/10.1039/b719557e.
18. Sakai S, Ohi H, Hotta T, *et al.*, 2018, Differentiation potential of human adipose stem cells bioprinted with hyaluronic acid/gelatin-based bioink through microextrusion and visible light-initiated crosslinking. Biopolymers, 109(2): e23080.

https://doi.org/10.1002/bip.23080.
19. Sakai S, Hirose K, Moriyama K, *et al.*, 2010, Control of cellular adhesiveness in an alginate-based hydrogel by varying peroxidase and H(2)O(2) concentrations during gelation. Acta Biomater., 6(4): 1446-1452.

https://doi.org/10.1016/j.actbio.2009.10.004.
20. Sakai S, Kamei H, Mori T, *et al.*, 2018, Visible Light-Induced Hydrogelation of an Alginate Derivative and Application to Stereolithographic Bioprinting Using a Visible Light Projector and Acid Red. Biomacromolecules, 19(2): 672-679.

https://doi.org/10.1021/acs.biomac.7b01827.
21. Jin R, Moreira Teixeira LS, Dijkstra PJ, *et al.*, 2009, Injectable chitosan-based hydrogels for cartilage tissue engineering. Biomaterials, 30(13): 2544-2551.

https://doi.org/10.1016/j.biomaterials.2009.01.020.
22. Hidaka M, Kojima M, Nakahata M, *et al.*, 2021, Visible Light-Curable Chitosan Ink for Extrusion-Based and Vat Polymerization-Based 3D Bioprintings. Polymers (Basel), 13(9): 1382.

https://doi.org/10.3390/polym13091382.
23. Sakai S, Tsumura M, Inoue M, *et al.*, 2013, Polyvinyl alcohol-based hydrogel dressing gellable on-wound via a co-enzymatic reaction triggered by glucose in the wound exudate. J Mater Chem B, 1(38): 5067-5075.

https://doi.org/10.1039/c3tb20780c.
24. Lim KS, Ramaswamy Y, Roberts JJ, *et al.*, 2015, Promoting Cell Survival and Proliferation in Degradable Poly(vinyl alcohol)-Tyramine Hydrogels. Macromol. Biosci., 15(10): 1423-1432.

https://doi.org/10.1002/mabi.201500121.
25. Hu M, Kurisawa M, Deng R, *et al.*, 2009, Cell immobilization in gelatin-hydroxyphenylpropionic acid hydrogel fibers. Biomaterials, 30(21): 3523-3531.

https://doi.org/10.1016/j.biomaterials.2009.03.004.
26. Sakai S, Ohi H, Taya M, 2019, Gelatin/Hyaluronic Acid Content in Hydrogels Obtained through Blue Light-Induced Gelation Affects Hydrogel Properties and Adipose Stem Cell Behaviors. Biomolecules, 9(8): 342.

https://doi.org/10.3390/biom9080342.
27. Ogushi Y, Sakai S, Kawakami K, 2007, Synthesis of enzymatically-gellable carboxymethylcellulose for biomedical applications. J. Biosci. Bioeng., 104(1): 30-33.

https://doi.org/10.1263/jbb.104.30.
28. Badali E, Hosseini M, Varaa N, *et al.*, 2022, Production of uniform size cell-enclosing silk derivative vehicles through coaxial microfluidic device and horseradish crosslinking reaction. Eur. Polym. J., 172: 111237.

https://doi.org/ARTN 111237

10.1016/j.eurpolymj.2022.111237.

29. Mu X, Sahoo JK, Cebe P, *et al.*, 2020, Photo-Crosslinked Silk Fibroin for 3D Printing. Polymers (Basel), 12(12): 2936.

https://doi.org/10.3390/polym12122936.
30. Prasetyaningrum PW, Mubarok W, Kotani T, *et al.*, 2025, Development of starch-based support material alternately extruded with gelatin-based bioinks for 3D bioprinting application. Bioprinting, 51: e00439.

https://doi.org/10.1016/j.bprint.2025.e00439.
31. Liang L, Li Z, Yao B, *et al.*, 2023, Extrusion bioprinting of cellular aggregates improves mesenchymal stem cell proliferation and differentiation. Biomater Adv, 149: 213369.

https://doi.org/10.1016/j.bioadv.2023.213369.
32. Pittenger MF, Mackay AM, Beck SC, *et al.*, 1999, Multilineage potential of adult human mesenchymal stem cells. Science, 284(5411): 143-147.

https://doi.org/10.1126/science.284.5411.143.
33. Mohand-Kaci F, Assoul N, Martelly I, *et al.*, 2013, Optimized hyaluronic acid-hydrogel design and culture conditions for preservation of mesenchymal stem cell properties. Tissue Eng Part C Methods, 19(4): 288-298.

https://doi.org/10.1089/ten.TEC.2012.0144.
34. Caiado Decarli M, Ferreira HP, Sobreiro-Almeida R, *et al.*, 2025, Embedding Bioprinting of Low Viscous, Photopolymerizable Blood-Based Bioinks in a Crystal Self-Healing Transparent Supporting Bath. Small Methods, 9(1): e2400857.

https://doi.org/10.1002/smtd.202400857.
35. Ning L, Mehta R, Cao C, *et al.*, 2020, Embedded 3D Bioprinting of Gelatin Methacryloyl-Based Constructs with Highly Tunable Structural Fidelity. ACS Appl Mater Interfaces, 12(40): 44563-44577.

https://doi.org/10.1021/acsami.0c15078.
36. Hinton TJ, Hudson A, Pusch K, *et al.*, 2016, 3D Printing PDMS Elastomer in a Hydrophilic Support Bath via Freeform Reversible Embedding. ACS Biomater Sci Eng, 2(10): 1781-1786.

https://doi.org/10.1021/acsbiomaterials.6b00170.
37. Deng Z, Nakagawa M, Zheng S, *et al.*, 2025, Induction of apoptosis for UE7T-13 cells using ultraviolet treatment. Journal of Osaka Dental University, 59(1): 191-198.
38. Chatree K, Sriboonaied P, Phetkong C, *et al.*, 2023, Distinctions in bone matrix nanostructure, composition, and formation between osteoblast-like cells, MG-63, and human mesenchymal stem cells, UE7T-13. Heliyon, 9(5): e15556.

https://doi.org/10.1016/j.heliyon.2023.e15556.
39. Takeda Y, Mori T, Imabayashi H, *et al.*, 2004, Can the life span of human marrow stromal cells be prolonged by bmi-1, E6, E7, and/or telomerase without affecting cardiomyogenic differentiation? J. Gene Med., 6(8): 833-845.

https://doi.org/10.1002/jgm.583.
40. Sakai S, Hirose K, Taguchi K, *et al.*, 2009, An injectable, in situ enzymatically gellable, gelatin derivative for drug delivery and tissue engineering. Biomaterials, 30(20): 3371-3377.

https://doi.org/10.1016/j.biomaterials.2009.03.030.
41. Sakai S, Kotani T, Harada R, *et al.*, 2022, Development of phenol-grafted polyglucuronic acid and its application to extrusion-based bioprinting inks. Carbohydr. Polym., 277: 118820.

https://doi.org/10.1016/j.carbpol.2021.118820.

42. Snyder J, Rin Son A, Hamid Q, *et al.*, 2015, Mesenchymal stem cell printing and process regulated cell properties. Biofabrication, 7(4): 044106.

https://doi.org/10.1088/1758-5090/7/4/044106.
43. Dong JD, Gu YQ, Li CM, *et al.*, 2009, Response of mesenchymal stem cells to shear stress in tissue-engineered vascular grafts. Acta Pharmacol Sin, 30(5): 530-536.

https://doi.org/10.1038/aps.2009.40.
44. Bai K, Huang Y, Jia X, *et al.*, 2010, Endothelium oriented differentiation of bone marrow mesenchymal stem cells under chemical and mechanical stimulations. J. Biomech., 43(6): 1176-1181.

https://doi.org/10.1016/j.jbiomech.2009.11.030.
45. Elvitigala K, Mubarok W, Sakai S, 2024, Hydrogels with Ultrasound-Treated Hyaluronic Acid Regulate CD44-Mediated Angiogenic Potential of Human Vascular Endothelial Cells In Vitro. Biomolecules, 14(5): 604.

https://doi.org/10.3390/biom14050604.
46. Mimura S, Kimura N, Hirata M, *et al.*, 2011, Growth factor-defined culture medium for human mesenchymal stem cells. Int. J. Dev. Biol., 55(2): 181-187.

https://doi.org/10.1387/ijdb.103232sm.
47. Demirel G, Cakil YD, Koltuk G, *et al.*, 2024, The use of hyaluronic acid in a 3D biomimetic scaffold supports spheroid formation and the culture of cancer stem cells. Sci Rep, 14(1): 19560.

https://doi.org/10.1038/s41598-024-69047-6.
48. Kim Y, Kumar S, 2014, CD44-mediated adhesion to hyaluronic acid contributes to mechanosensing and invasive motility. Mol. Cancer Res., 12(10): 1416-1429.

https://doi.org/10.1158/1541-7786.MCR-13-0629.
49. Sano M, Mine Y, Okazaki S, *et al.*, 2025, Deep learning predicts osteogenic differentiation stages of human mesenchymal stem cells from phase-contrast microscopy images. Dent Mater J, 44(5): 557-563.

https://doi.org/10.4012/dmj.2025-015.
50. Edwards SD, Ganash M, Guan Z, *et al.*, 2024, Enhanced osteogenesis of mesenchymal stem cells encapsulated in injectable microporous hydrogel. Sci Rep, 14(1): 14665.

https://doi.org/10.1038/s41598-024-65731-9.
51. Duarte Campos DF, Blaeser A, Buellesbach K, *et al.*, 2016, Bioprinting Organotypic Hydrogels with Improved Mesenchymal Stem Cell Remodeling and Mineralization Properties for Bone Tissue Engineering. Adv Healthc Mater, 5(11): 1336-1345.

https://doi.org/10.1002/adhm.201501033.
52. Ogushi Y, Sakai S, Kawakami K, 2013, Adipose tissue engineering using adipose-derived stem cells enclosed within an injectable carboxymethylcellulose-based hydrogel. J Tissue Eng Regen Med, 7(11): 884-892.

https://doi.org/10.1002/term.1480.
53. Bian L, Hou C, Tous E, *et al.*, 2013, The influence of hyaluronic acid hydrogel crosslinking density and macromolecular diffusivity on human MSC chondrogenesis and hypertrophy. Biomaterials, 34(2): 413-421.

https://doi.org/10.1016/j.biomaterials.2012.09.052.
54. Machour M, Hen N, Goldfracht I, *et al.*, 2022, Print-and-Grow within a Novel Support Material for 3D Bioprinting and Post-Printing Tissue Growth. Adv Sci (Weinh), 9(34): e2200882.

https://doi.org/10.1002/advs.202200882.

55. Poveda-Reyes S, Moulisova V, Sanmartin-Masia E, *et al.*, 2016, Gelatin-Hyaluronic Acid Hydrogels with Tuned Stiffness to Counterbalance Cellular Forces and Promote Cell Differentiation. Macromol. Biosci., 16(9): 1311-1324.

https://doi.org/10.1002/mabi.201500469.
56. McAndrews KM, McGrail DJ, Quach ND, *et al.*, 2014, Spatially coordinated changes in intracellular rheology and extracellular force exertion during mesenchymal stem cell differentiation. Phys Biol, 11(5): 056004.

https://doi.org/10.1088/1478-3975/11/5/056004.